9/3

LBL-10832 c.2
Preprint

Lawrence Berkeley Laboratory
UNIVERSITY OF CALIFORNIA

Materials & Molecular Research Division

RECEIVED
LAWRENCE
BERKELEY LABORATORY
SEP 8
LIBRARY
DOCUMENTS SECTION

Submitted to the Journal of Applied Physics

SEGREGATION IN CZOCHRALSKI GROWN CALCIUM GALLIUM GERMANIUM GARNET SINGLE CRYSTALS

T.F. Roth, R.K. Mishra, and G. Thomas

July 1980

TWO-WEEK LOAN COPY

This is a Library Circulating Copy which may be borrowed for two weeks. For a personal retention copy, call Tech. Info. Division, Ext. 6782

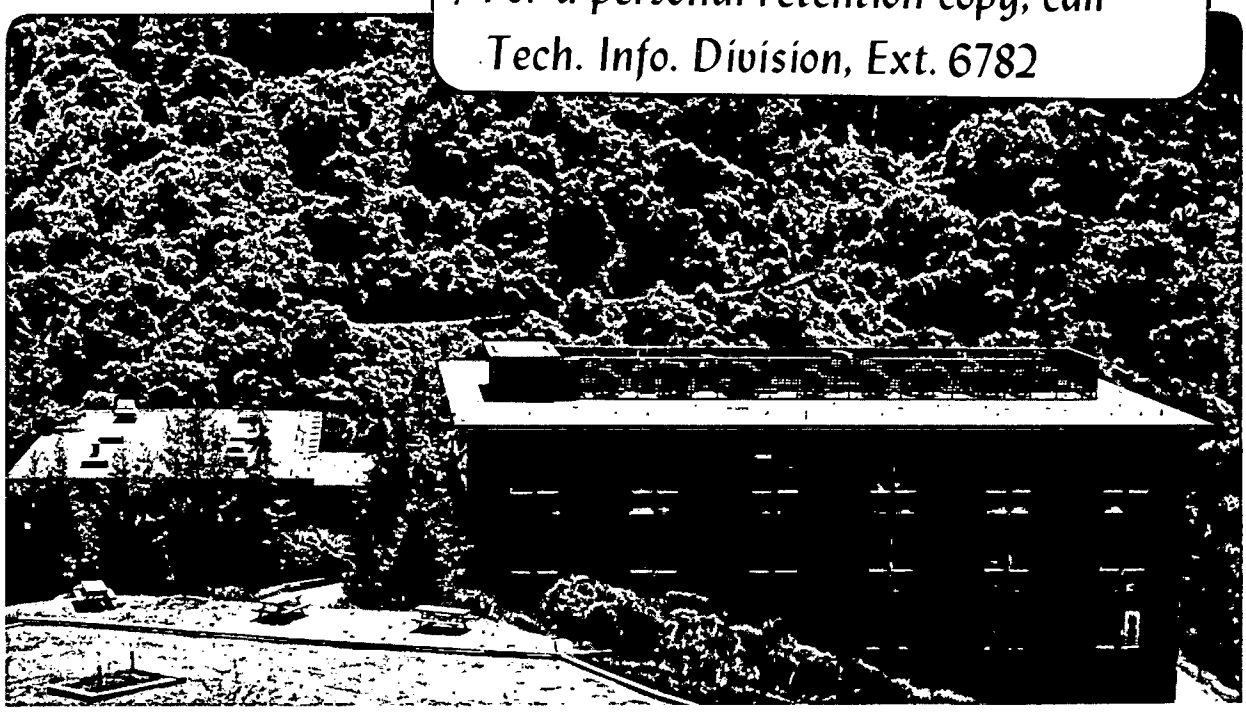

Prepared for the U.S. Department of Energy under Contract W-7405-ENG-48

LBL-10832 c.2

DISCLAIMER

This document was prepared as an account of work sponsored by the United States Government. While this document is believed to contain correct information, neither the United States Government nor any agency thereof, nor the Regents of the University of California, nor any of their employees, makes any warranty, express or implied, or assumes any legal responsibility for the accuracy, completeness, or usefulness of any information, apparatus, product, or process disclosed, or represents that its use would not infringe privately owned rights. Reference herein to any specific commercial product, process, or service by its trade name, trademark, manufacturer, or otherwise, does not necessarily constitute or imply its endorsement, recommendation, or favoring by the United States Government or any agency thereof, or the Regents of the University of California. The views and opinions of authors expressed herein do not necessarily state or reflect those of the United States Government or any agency thereof or the Regents of the University of California.

SEGREGATION IN CZOCHRALSKI GROWN CALCIUM GALLIUM GERMANIUM GARNET SINGLE CRYSTALS

T.F. Roth*, R.K. Mishra and G. Thomas

Materials and Molecular Research Division
Lawrence Berkeley Laboratory, and
Department of Materials Science and Mineral Engineering,
University of California, Berkeley, CA 94720

*IBM, San Jose, CA 95193

ABSTRACT

Morphology and crystallography of the formation of small segregates in Czochralski grown calcium gallium germanium garnet (CGGG) are studied using TEM and STEM. Based on the observations, the following model has been developed for the formation of these defects. Evaporative loss of Ge from the melt during the crystal growth and the resulting local deviations from stoichiometry lead to random nucleation of small plate-like precipitates, rich in Ga. As these precipitates grow, strain field interaction leads first to the formation of three-dimensional segregates and later, to their alignment along the elastically soft <100> directions. Isolated segregates are also observed. Some of the segregates contain a central void filled with oxygen gas while some others with or without a void have one or more dislocation loops around them. These segregates have the same garnet structure, but a different chemical composition; rich in Ga and depleted in Ge. The model suggests that segregate-free crystals can be grown by suppressing the evaporative loss of Ge from the melt during crystal growth.

I. INTRODUCTION

The advantages of Calcium Gallium Germanium Garnet ($Ca_3Ga_2Ge_3O_{12}$ or CGGG) over Gadolinium Gallium Garnet ($Gd_3Ga_5O_{12}$ or GGG) as a substrate material for magnetic bubble films has already been shown.[1] Although CGGG single crystal boules have been grown successfully, the defect densities in CGGG are higher that those obtained in GGG crystals. Since a prerequisite for the growth of a defect free epitaxial film is a defect free substrate,[2] it is necessary to identify the defects that exist in CGGG in order to optimize processing parameters for their elimination. In the present investigation, defects found in Czochralski grown CGGG single crystals have been identified and characterized with respect to their distribution, structure, morphology, and composition using transmission electron microscopy and chemical analysis. Based on these observations, a model to explain the formation of these defects has been developed.

II. EXPERIMENT

The CGGG single crystals used in this study were grown at Philips Laboratories of Eindhoven, Netherlands, from a starting powder mixture with Ca:Ga:Ge = 73.2:24.8:38 (atomic ratios). Details of the crystal growth can be found in Reference 1. Specimens for transmission electron microscopy were prepared by mechanical polishing, followed by ion-milling from thin slices cut from the boule. It was necessary to deposit a thin layer of carbon on the thin specimens to avoid electrostatic charge build-up in the electron microscope. The specimens were examined in a Hitachi HU-650 high voltage electron microscope operating at 650kV. Chemical microanalysis was done in a Philips 400 electron microscope with a 200Å probe of 120kV electrons at Rockwell Science Center, Thousand Oaks, California.

III. RESULTS AND INTERPRETATION

a) Chemical Defects or Microsegregates

Commonly observed defects in the CGGG samples are small regions of chemical inhomogeneity.[1] These can be identified easily by their dark contrast against the lighter matrix in TEM micrographs. Two closely-spaced defects of this type are imaged in Fig. 1. The interface between the defective region and the matrix is sharp and shows no evidence of dislocations despite being obscured by the encircling periodic lobes of intensity. The lobes are also seen to overlap in the region between the two chemical defects where the periodic intensity variations are interrupted. Lobed "butterfly" contrast of this sort is generally attributed to a coherent lattice imperfection which strains the matrix.[3] The projected shape of each inhomogeneity is approximately elliptical with major and minor axes of lengths 0.25μ and 0.20μ, respectively. Bright field stereomicrographs confirm these defects to be ellipsoidal.

Another commonly observed morphology of the chemical inhomogeneities is shown in Fig. 2. These defects also appear dark, but they include a light circular patch, central to their interiors. The matrix-defect interface is well-defined, and no strain contrast is observed. The interface is generally curved, but faceted interfaces are also seen, Fig. 2b. Stereomicroscopy establishes that these defects are roughly cylindrical in shape with an irregular cross-sectional area. The light patch is spherical in shape and lies near the center of the cylinder. Dislocations, such as the ones at d in Fig. 2b, are commonly seen lying only in the matrix around these defects.[4]

These defects show the same dark contrast both in the bright field and dark field images, and so does the central circle, which shows light contrast. The electron diffraction patterns from the defects are identical to those from the matrix, indicating that the defects have a structure identical to and lattice parameter similar to that of the matrix. This has been confirmed by extensive tilting and dark field experiments.

The defects tend to be localized. In regions of relatively high defect density, the chemically inhomogeneous regions are distributed at random as well as in linear arrays. Figures 3a and 3b show adjacent regions in a [001] oriented CGGG specimen. Linear arrays are observed aligned parallel to the mutually perpendicular <100> crystallographic directions in the plane of the specimen. Although arrays aligned parallel to <110> were also observed in some areas, alignment parallel to <100> was much more common. Inhomogeneities with and without the central sphere occur in these arrays. In Fig. 3a, a chemical defect with a central sphere is seen at S. This defect is bounded by semicircular arcs having a line of no contrast perpendicular to the operating $\vec{g}$, due to a prismatic edge dislocation loop around the defect. Such dislocation loops are discussed in detail later.

The nature of the matrix/defect interface can be considered to be coherent for inhomogeneities showing strain contrast, and coherency is partially lost when dislocations are generated in the matrix near the interface.

Observation of strain fields around some of the defects can be correlated with the linear alignment of the chemical defects. Alignment of precipitate particles has been reported in other systems[5] where the transformation of one particle tends to cause the transformation of neighboring particles

along certain crystallographic directions. An elastic interaction between the chemical inhomogeneities is likely since they are separated by distances comparable to their diameter and evidence of overlapping strain fields has in fact been observed. (Figs. 1 and 3).

Considering the interaction of dilatational strains in elastically anisotropic cubic crystals, it can be shown[6] that it is energetically favorable to nucleate a second particle in an elastically soft direction. Thus, in such a system, free energy considerations will favor growth of the particles in linear arrays, even if they nucleate randomly. The <100> directions are favored if $(2C_{44}-C_{11}+C_{12}) > 0$, as is the case with garnet structure compounds.[7] Thus, it is possible that the observed alignment of the defects occurs during growth, whose driving force is derived from strain energy.

The light contrast displayed in both BF and DF by the spherical feature central to some of the chemical inhomogeneities indicates that the sphere is composed of material which allows greater electron transmittance. The spherical morphology is indicative of a hydrostatic pressure such as that exerted by entrapped gas.

Chemical microanalysis was performed for both the matrix and the different kinds of inhomogeneities using energy dispersive X-ray spectral analysis in the STEM. Fig. 4 shows the traces of the spectra obtained from the matrix and defect regions.

Qualitative analysis of the K_α peaks of the resulting spectra from defects with and without the central sphere shows several consistent results. All matrix and defect regions show evidence of only five elements, those being Ca, Ga, Ge, and smaller amounts of Fe and Cu, the later two coming

from the background spectra. No oxygen is detected due to the limitation of the resolution of STEM/EDX unit. All defect spectra show the relative heights of the K_α peaks for Ga and Ge to be reversed with respect to their corresponding matrix spectra, i.e., the defects have more Ga than Ge and vice versa for the matrix. Spectra obtained with the probe placed central to the spheres show inconsistent and uninterpretable behavior.

For quantitative chemical analysis,[8] the three following assumptions are made: (1) the area under a peak for a given element is directly proportional tc the number of atoms of that element present in the volume of material from which chemical information is being received, (2) the matrix material is stoichiometric $Ca_3Ga_2Ge_3O_{12}$, and (3) the defective region is a garnet of composition $Ca_xGa_yGe_zO_{12}$ where $x+y+z = 8$. Following the method of Goldstein et al.,[8] by taking the appropriate ratios of areas under the peaks from matrix regions and comparing with the stoichiometric cation atomic fraction ratios, it is possible to deduce a nominal composition of the defective regions from the ratios of the area under their STEM/EDAX spectra peaks.

The calculated composition $Ca_xGa_yGe_zO_{12}$ of 4 different chemically defective regions is given in Table 1. The nominal composition of chemical defects having spheres (STEM 3 and 6) is very comparable to that of defects not having a sphere (STEM 9 and 11). All defects show the composition $Ca_xGa_yGe_zO_{12}$ to be rich in gallium and depleted in germanium relative to the $Ca_3Ga_2Ge_3O_{12}$ matrix. The calcium content of both matrix and defect seems similar. By simply taking an arithmetic average of the x,y, and z parameters a nominal composition of the chemically inhomogeneous material is found to be $Ca_{3.12}Ga_{3.39}Ge_{1.48}O_{12}$. This composition is subject to the

limitations of the instrument and the analytical method[9], as well as the above three assumptions. There also arises uncertainty in the composition of the inhomogeneities since they lie central to the depth of the sample. X-ray spectra are thus likely to have also been obtained from columns of matrix material between the specimen surface and the defect interface and not uniquely from the chemical defect itself.

Nevertheless, the chemical information obtained shows several significant features. Chemical inhomogeneities with and without spheres are undoubtedly related phenomena as indicated by the similarity in their elemental composition, as well as their size, shape, distribution and contrast behavior. In addition, both result from interactions among chemical species intrinsic to the CGGG system, i.e. Ca, Ga, and Ge and not any other impurities. The chemical defects are formed as a result of small scale segregation of gallium in the garnet structure. These microsegregates, as they may be referred to henceforth, are depleted in germanium, enriched in gallium, and equivalent in calcium content relative to the $Ca_3Ga_2Ge_3O_{12}$ matrix.

A garnet having composition $Ca_{3.12}Ga_{3.39}Ge_{1.48}O_{12}$ would have a larger lattice parameter than $Ca_3Ga_2Ge_3O_{12}$ since garnets obey Vegard's rule[10] and the ionic radius of Ga^{3+} is larger than that of Ge^{4+} by about 0.09Å. A rough estimation shows that the microsegregates have a = 12.38Å (compared to 12.252Å for CGGG matrix).[11]

To maintain electroneutrality a garnet of composition $Ga_{3.12}Ga_{3.39}Ge_{1.48}O_v$ would need 8x(3.12x2 + 3.39x3 + 1.48x4) = 178 units of negative charge per unit cell (v = 11.17). This could be supplied by only eighty-nine O^{2-} ions, and there would be surplus oxygen in a region of such a garnet phase

if the normal ninety six oxygens per garnet unit cell are available. This surplus oxygen could be involved in the formation of the oxygen filled sphere, with the accumulation of oxygen motivated by electrostatic imbalance as the crystal cools.

It has been reported that evaporative loss of germanium occurs during crystal growth.[1] It is possible that as germanium evaporates, for whatever reason, gallium segregates to occupy the tetrahedral sites as well as their normal octahedral sites in the garnet structure.[10] It is likely that such sites in CGGG would easily accommodate the Ga^{3+} ions since oxygen packing around tetrahedral sites is less dense than the packing around octahedral sites. Calcium, being the largest cation, cannot fit into octahedral nor tetrahedral interstices and it is not suprising that calcium occupancy of dodecahedral sites is maintained in the microsegregated regions.

b) Dislocations

Dislocations in the CGGG samples tended to be in close physical proximity to the microsegregates. Although isolated matrix dislocation loops such as those reported by Mishra and Thomas[4] were also observed, the density of dislocations not associated with the chemical defects was low. A common configuration of dislocations is illustrated in Fig. 5. A microsegregate with a sphere is imaged in bright field under three different diffracting conditions. Two mutually perpendicular dislocation loops about 0.5μ in diameter and lying in the matrix encircle the defective region in Fig. 5a. Trace and $\vec{g}\cdot\vec{b}$ contrast analyses reveal such dislocation loops to be of edge type and no evidence of dissociation of the loops into partial dislocations is seen. The Burgers vector of each

loop is of magnitude a_o <100> and is perpendicular to the {100} plane on which the loop lies.

Another example of such loops encircling a chemical defect with a sphere is seen in the weak-beam dark field micrograph of Fig. 6. The view is parallel to $[1\bar{2}0]$ and one loop on (001) is seen edge-on while evidence of multiple dislocation images on the orthogonal (010) plane can be seen at d. No evidence of intensity fringes can be seen between the multiple images. The edge-on loop has a Burgers vector of a_o <001> perpendicular to the plane of that loop. Although the Burgers vectors of the dislocations at d were not definitively established, they are not parallel to <010>.

The double dislocation image of region d of Fig. 6 can be interpreted as (1) a double image of a single dislocation line, (2) one image each of two different concentric loops, or (3) two partial dislocations separated by a region of stacking fault.

The possibility that the double dislocation image arises from a single dislocation must not be overlooked. Mishra and Thomas[4] have shown through calculations of theoretical image profiles that double images of a single undissociated dislocation can still arise despite the increased resolution obtained from weak-beam dark-field imaging. Burgers vectors other than a_o <001> also have been reported earlier.[4]

Dislocations near the microsegregates act to relieve strain due to lattice mismatch between the garnet structures of the matrix and the microsegregates. This is suggested by the fact that all dislocations were found to lie primarily in the matrix and is apparent from the reduced matrix strain contrast associated with dislocated microsegregates. It

is possible that the dislocation loops always lie in the matrix material and are later attracted to the region of the growing chemical inhomogeneity. Under this circumstance it might be expected that matrix dislocations would be seen in the vicinity of the strained chemical defects (not having central spheres) and these are seldom observed experimentally. Instead, it is more likely that dislocations are generated by the growing microsegregates.

The dislocation loops of Figs. 5 and 6 are found to encircle the microsegregates and lie in the matrix material several hundered angstroms away from the interface. This suggests that the dislocation accommodates matrix strain and that while the dislocation may have been generated at the interface it has grown into the matrix by climb. These loops lying on {001} planes are seen face-on in region S in the plane of the {001} oriented foil of Fig. 3 a and give rise to the split-ring image typical of edge dislocation loops.

Mechanisms for dislocation loop generation in GGG around chemical inhomogeneities have been proposed by J.W. Matthews[12] and it is possible that some of those mechanisms operate in this case. These will not be discussed further here.

Another distinct defect configuration commonly encountered can be shown in Fig. 7. These look like small loops or platelets about 0.1μ in size and are not physically associated with established microsegregate defects. Contrast from the interior of such platelets is not clear.

Contrast from these plate-like features is very sensitive to diffracting conditions such as the particular operating reflection excited and the deviation parameter s. Stereomicroscopy shows these

platelets to be distributed fairly uniformly throughout the thickness of the specimen. Selected area diffraction patterns from the areas of the sample where the small platelets are profilic do not contain extra spots, streaks, or other anomalies not resolved in S.A.D. patterns obtained from undefective CGGG matrix.

Despite meticulous tilting of the specimen, the small platelets could not be made to go completely out of contrast. Plates viewed face-on commonly show a line of no contrast through the platelet in a direction perpendicular to the operating diffraction vector $\vec{g}$ (Fig. 7A). Stereographic analysis of face-on and edge-on plates in the [001] oriented specimen of Fig. 7A showed the platelets to be lying on {001} type planes, however, similar analysis of other platelets indicated that alternative habit planes are also likely.

Several of the small platelets can be seen in very close proximity to each other in region C of Fig. 7B. Stereomicroscopy of these platelets indicates that coalescence of the platelets into a three-dimensional feature has occurred.

Contrast from the small plate-like features indicates that they may be either dislocation loops or else coherent or partially coherent precipitates. Distinguishing between these various possible defects is sometimes difficult on the basis of contrast phenomena alone. However, qualitatively it is easier to explain formation of three-dimensional defects in terms of coalescence of precipitates rather than dislocations. Also, prismatic loops might be expected to show very weak or zero contrast in some diffraction conditions where $\vec{g}\cdot\vec{b} = 0$, and no reflection was found which caused virtual disappearance of any of these features. Consequently,

it is assumed that they may be coherent or partially coherent precipitates.[13]

Several factors indicate that the small plate-like precipitates are related to the larger microsegregate defects. Specimens often contain both types of defects except in different areas which are usually separated by regions of undefective matrix. Both types of defects are observed in the bulk of the specimens suggesting that they are defects intrinsic to CGGG and not specimen preparation artifacts. The {100} habit plane of the small precipitates is reminiscent of the {100} habit plane of the large edge dislocation loops surrounding the microsegregates with spheres. These precipitates could conceivably act as nucleation sites for the small climb loops of Matthews' theory.[12] In addition, the observed coalescence of several precipitates into a three-dimensional mass indicates that the precipitates are a preliminary stage in the formation of the larger microsegregate defects. Evidence of the growth of a linear array of the segregates from these loop-like precipitates is shown in Fig. 8, where the platelets have been consumed from the denuded zone[5] on either side of the array during the growth of the segregates.

Chemical microanalysis was done using STEM/EDX by placing a 200Å diameter probe of 120keV electrons central to a face-on platelet and comparing the chemical information thus obtained with information from undefective CGGG matrix regions. These precipitates show no evidence of elements extrinsic to the CGGG system (except Fe and Cu as explained previously), but the resolvable difference in the composition of the matrix and the precipitate is negligible.

The pocked appearance of the matrix around the small loops displays contrast effects characteristic of point defect clusters. The small

"points" reverse contrast across extinction contour and in BF/DF image pairs. In addition, Fig. 7B shows the points to have a black-white lobe contrast, with the direction $\vec{q}$ of white to black contrast aligned both parallel or antiparallel to the operating $\vec{g}$. These point defect clusters are seen only in regions containing the platelets, not the microsegregates, discussed earlier.

IV. DISCUSSION

As pointed out already, although the microsegregates and the plate-like precipitates occur in the same sample in different parts, they are related. In fact, they are manifestations of the same phenomenon at different stages of its development. A model of microsegregate formation entailing nucleation and successive stages of growth, which corresponds to these observed results is suggested below.

Defect formation commences with the random nucleation of the small plate-like precipitates shown in Fig. 7. This occurs due to the preferential evaporative loss of Ge from the melt and results in local deviations from stoichiometry. Evaporation rate is sensitive to temperature[1] (and oxygen partial pressure) and consequently thermal fluctuations in the melt solution can be responsible for localized germanium loss. As the germanium is lost through evaporation the small loop-like second garnet phase is formed by incorporating Ga^{3+} ions in sites of the growing crystal which would normally be occupied by Ge^{4+} ions.

The subsequent growth of the coherent loop-like precipitates generate strain fields around the precipitates. Continued growth and interaction of overlapping strain fields then enhance coalescence of closely spaced individual precipitates into a larger chemical defect, as is indicated in region C of Fig. 7B. The result of such coalescence of small plate-like

precipitates is the larger strained chemically inhomogeneous regions (without the central sphere) as is seen in Figs. 1 and 3.

Coalescence of small precipitates into the larger, strained chemical defects continues until the population of the larger defects is great enough and their physical separation small enough to permit interaction of overlapping strain fields. Strain field interactions then motivate the alignment of the defects along crystallographically soft directions as dictated by the anisotropic elastic constants of the material. This notion of formation of larger chemical defects from the coalescence of smaller plate-like precipitates and their subsequent alignment due to strain is consistent with the observations of Fig. 8.

The above stages in the formation of the segregates and the succession of events leading to further formation of the internal oxygen filled sphere and/or encircling dislocation loop can occur simultaneously during crystal growth or upon further cooling. Formation of a single dislocation loop could occur by the method of Matthews[14]. This method requires formation of a small prismatic loop outside of the microsegregate. Such small prismatic loops have been observed to nucleate around small precipitates in other systems[15,16] and the small plate-like precipitates found in CGGG are suspected to act as nucleation sites. The loop is nucleated due to strain, which is enhanced upon cooling, and grows to successively larger diameters by climb. Size of the microsegregate defect does not seem to be the only critical factor in loop formation since relatively large (0.6μ) as well as small (0.2μ) microsegregates have been observed with and without encircling loops. Instead, strain energy per unit volume is suspected as a critical factor since it is independent of size.

Generation of the mutually perpendicular loops seen in Fig. 5 requires only that the individual loops nucleate around small precipitates lying on mutually perpendicular {100} planes. Three mutually perpendicular loops on {100} could conceivably encircle a microsegregate. This is not observed experimentally since one of the <100> was coincident with the crystal pulling/rotation axis during growth of the CGGG boule.

Formation of the oxygen-filled sphere is likely to accompany or follow relief of microsegregate strain since microsegregates with the central sphere seldom show pronounced strain contrast. The oxygen within the sphere can be supplied by the constituent garnet oxides of the melt or the imposed oxygen partial pressure of 760 torr above the melt solution. Since the size of the sphere is related to the size of the microsegregate in which it is found (i.e., the diameter of the sphere is always about one third of the largest dimension of the microsegregate) the oxygen is probably supplied from the melt solution in the following way. The evaporation of Ge permits accommodation of Ga^{3+} ions on tetrahedral sites of the gorwing crystal normally occupied by Ge^{4+} ions. This substitution results in a metastable phase at the growth temperature since the size of Ge^{4+} and Ga^{3+} ions do not vary greatly and hence small strains are involved. In the regions where Ga^{3+} has been substituted for Ge^{4+}, there would be a deficiency of positive charge. This can be remedied by supplying additional positive charges or eliminating some negative charge. Supplying positive charge is not feasible since this is most easily accomplished using the Ge^{4+} ions which evaporate. Instead, negative charges are deleted by the leaching out of O^{2-} anions as the crystal cools. Accumulation of these anions occurs to form the oxygen filled sphere whose shape is maintained by the pressure of the accumulated oxygen gas.

From this model it is suggested that defect formation could depend upon evaporative loss of Ge from the melt. Thermal conditions in the melt solution and growth atmosphere have been shown to influence the rate of loss of Ge.[1] Consequently, any effort to eliminate the microsegregate defects must address these factors. Thermal fluctuations within the melt would be minimized by controlling heat loss from the crucible as well as by eliminating the unstable convective currents in the growth melt solution due to specimen wobble during rotation. Germanium loss due to evaporation may be reduced by imposing a higher GeO partial pressure above the melt (instead of O_2 only). The vapor pressure of Ge and GeO_2 above their pure substances near the CGGG crystal growth temperature are of the order of 10^{-3} torr. However, GeO is a substantially more volatile component with vapor pressures exceeding 760 torr at 1000°C.[17] Thus, germanium loss from the melt may be due to the volatility of GeO at high temperatures and imposing a GeO atmosphere above the melt may reduce the rate of germanium loss. The deposition of GeO_2 on the crystal pulling shaft[1] probably results by reaction of GeO gas upon cooling in the imposed oxygen atmosphere.

ACKNOWLEDGEMENTS

The authors wish to acknowledge J.P.M. Damen and J. Pistorius of Philips Research Laboratory, Eindhoven for providing the CGGG crystals as well as helpful suggestions, and D.R. Clarke of Rockwell Science Center, Thousand Oaks, CA for his help in the chemical microanalysis. Financial support from the DOE under Contract W-7405-ENG-48 is gratefully acknowledged.

REFERENCES

1. J.P.M. Damen, J.A. Pistorius nad J.M. Robertson, Mat. Res. Bull., 12, 1977, 73-78.

2. P. Chaudhuri, J.J. Cuomo, R.J. Gambino and E.A. Giess, Physics of Thin Films, 1, 1977, 263-297.

3. P.B. Hirsch, R.B. Nicholson, A. Howie, D.W. Pashley and M.J. Whelan, Electron Microscopy of Thin Crystals, Butterworth's, London, (1965), 96-7, 328-32.

4. R.K. Mishra and G. Thomas, J. Appl. Phys., 49, 1876-78 (1978).

5. H.F. Merrick and R.B. Nicholson, 5th Int. Cong. for Electron Micros., Vol. 1, K8, Academic Press, N.Y., 1962.

6. J.W. Cahn, from The Mechanisms of Phase Transformations in Crystalline Solids, Inst. of Metal, London, 1969, 1.

7. Londolt-Bornstein Tables, New Series, Group III, Vol. 1, p. 10 and Vol. 2, p.6-7, Springer-Verlag, N.Y., 1966.

8. J.I. Goldstein, J.L. Costley, G.W. Lorimer and S.J.B. Reed, Scanning Electron Microscopy, 1977, 1, 315-24.

9. N.J. Zaluzec in Introduction to Analytical Electron Microscopy, ed. J.J. Hren, J.L. Goldstein and D.C. Joy, (Plenum Press, 1979), p. 121.

10. J.E. Davies and E.A. Geiss, J. of Mat. Sci., 10, 1975, 2156.

11. ASTM X-Ray Powder File Index Card #11-23.

12. J.W. Mathews, Phys. Stat. Sol. (a) 15, 1973, 607.

13. G. Thomas in Modern Diffraction and Imaging Techniques in Materials Science, ed. S. Amelinckx, R. Gevers, G. Remant and J. Van Landuyt, North Holland Publishing Co., 1970.

14. J.W. Mathews, E. Klokholm and T.S. Plaskett, Phys. Stat. Sol. (a) 28, 1975, 95.

15. A. Eikum and G. Thomas, Acta Met. 12, 1964, 537.

16. K.H. Westmacott, R.S. Barnes and R.E. Smallman, Phil. Mag. 7, 1962, 1585.

17. V.I. Davydov, Germanium, Gordon & Breach, N.Y., 1966, 144-187.

FIGURE CAPTIONS

Fig. 1 Two closely spaced chemical defects about 0.25μ in size are seen as dark oval areas against a lighter CGGG matrix in these BF images. In the sequence ABCD the specimen was tilted to make the diffraction vector $\vec{g}$ rotate clockwise. The lobed contrast distorts to "follow" the operating reflection in a manner typical of strain contrast. Qualitative analysis of these strain effects, accounting for the overlap of strain fields from the two closely spaced defects, shows these are each ellipsoidal in shape.

Fig. 2a Microsegregate defects in CGGG are commonly 0.2-0.6μ in size and consist of a dark halo surrounding a light circular patch. The defect/matrix interface is quite sharp and appears curved in this bright field image.

Fig. 2b A microsegregate in a thin area of a CGGG specimen, imaged in bright field. The light central patch is seen to intersect the specimen surfaces leaving the inner annulus S, and reaches its widest equitorial dimension at M near the middle of the foil. This is consistent with this feature being spherical in shape. Dislocations are seen in contact with the interface at the regions designated d.

Fig. 3 Microsegregates with and without central spheres are commonly interspersed in linear arrays along <100> directions as seen in this pair of bright field micrographs from adjacent areas in a [001] oriented specimen. Note the split dislocation ring contrast of region S in Fig. 5a having a line of no contrast

perpendicular to $\vec{g}$. The region L of Fig. 3b shows strain field overlap among defects not having developed central spheres. The features marked K are cracks.

Fig. 4 Tracing of EDX spectra obtained from matrix and defect are seen in A and B, respectively. The K_α peaks are marked and show that only intrinsic to $Ca_3Ga_2Ge_3O_{12}$ were found, except for Fe and Cu which arise from the iron pole pieces of the microscope and copper grid upon which the specimen was mounted. Oxygen was not detectable using this technique.

Fig. 5 A microsegregate with a sphere in a [001] oriented CGGG specimen is imaged in there different diffracting conditions. In A, two mutually perpendicular dislocation loops are seen to surround the segregate while in each of B and C the crystal is tilted to make each of the loops go out of contrast in turn. The loops lie on {100} planes with Burgers vector perpendicular to the plane of the loop. Note that the loops lie in the matrix, away from the segregate.

Fig. 6 In this WBDF micrograph, an isolated segregate in a <120> oriented specimen has been imaged and the spherical void and dislocation loops on {100} planes are visible. Note the two dislocation loop images in the region marked d. It is suspected that this is not a double image of a single loop because of the weak beam conditions used to form the image. Instead, this is evidnece of either two concentric and coplanar perfect dislocation loops or a single dislocation loop which has dissociated into partials.

lying on a {100}.

Fig. 7 Small plate-like precipitates 0.1μ or less in size are imaged in bright field and weak beam dark field in A and B, respectively. The smallplate-like precipitates in a [001] oriented specimen are seen face-on as well as edge-on in A. Trace analysis reveals the precipitates to lie on {001} planes. The size and contrast (i.e. line of no contrast LC perpendicular to $\vec{g}$) indicate these to be coherent precipitates with resulting lattice displacements normal to their plane. Evidence of coalescence of several closely spaced precipitates can be seen in region C of (B). The pocked appearance of the matrix shows black/white contrast dependent on $\vec{g}$ and the mode of imaging (i.e. BF or DF) indicative of point defect clusters.

Fig. 8 Smallplate-like precipitates 0.1μ or less in diameter are seen in the vicinity of the larger (0.5μ) microsegregates, some of which show evidence of the light spheres displaced from their centers. Note the denuded region on either side of the larger microsegregates, suggesting the smallplate-like precipitates to be a preliminary stage in the formation of the larger chemical defects. The foil normal is along [001].

TABLE I.
MICROSEGREGATE COMPOSITION RESULTS

Run #	Description	Composition $Ca_xGa_yGe_zO_{12}$		
		x	y	z
STEM 3	Microsegregate with internal sphere	3.1452	3.8278	1.02711
STEM 6	Another microsegregate with internal sphere	2.965	2.9185	2.1163
STEM 9	Microsegregate without a sphere	3.2009	3.7047	1.0944
STEM 11	Another microsegregate without a sphere	3.1498	3.1257	1.6675

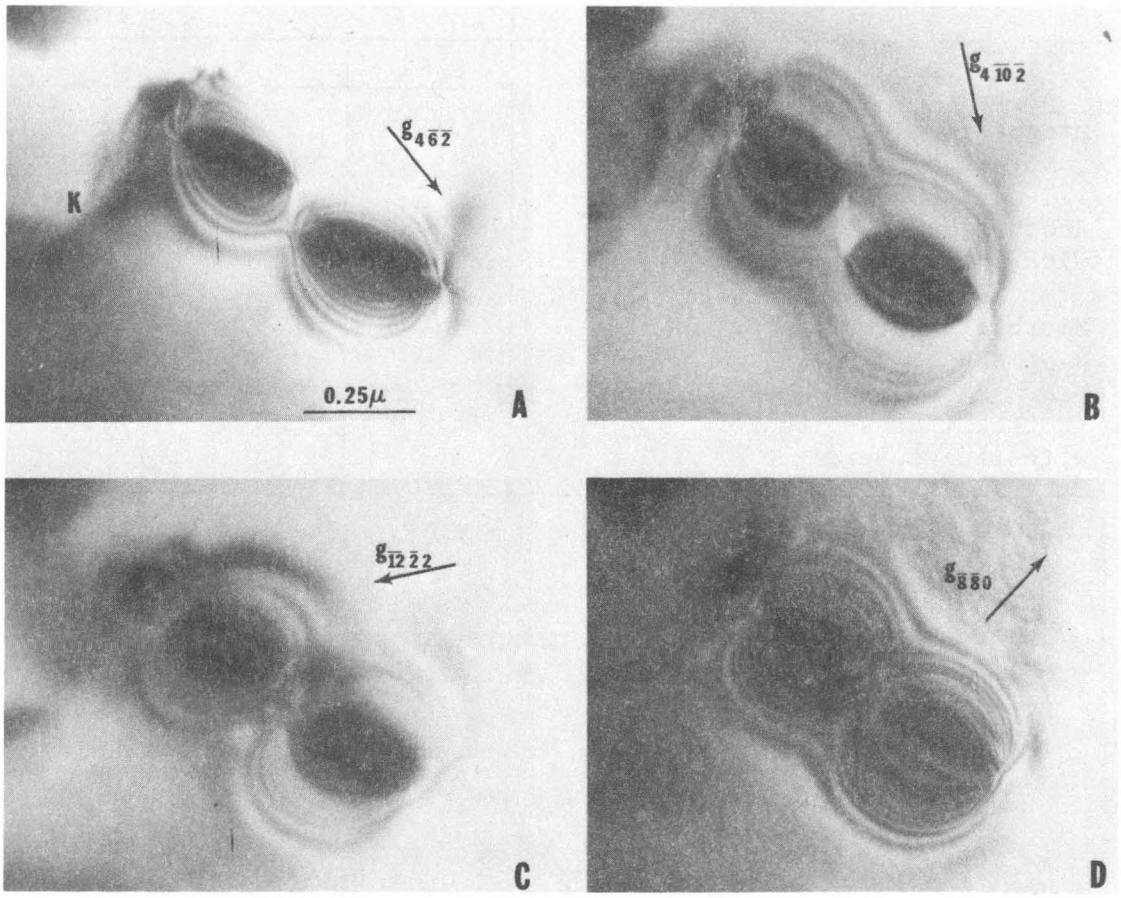

XBB 784-4979

Fig. 1

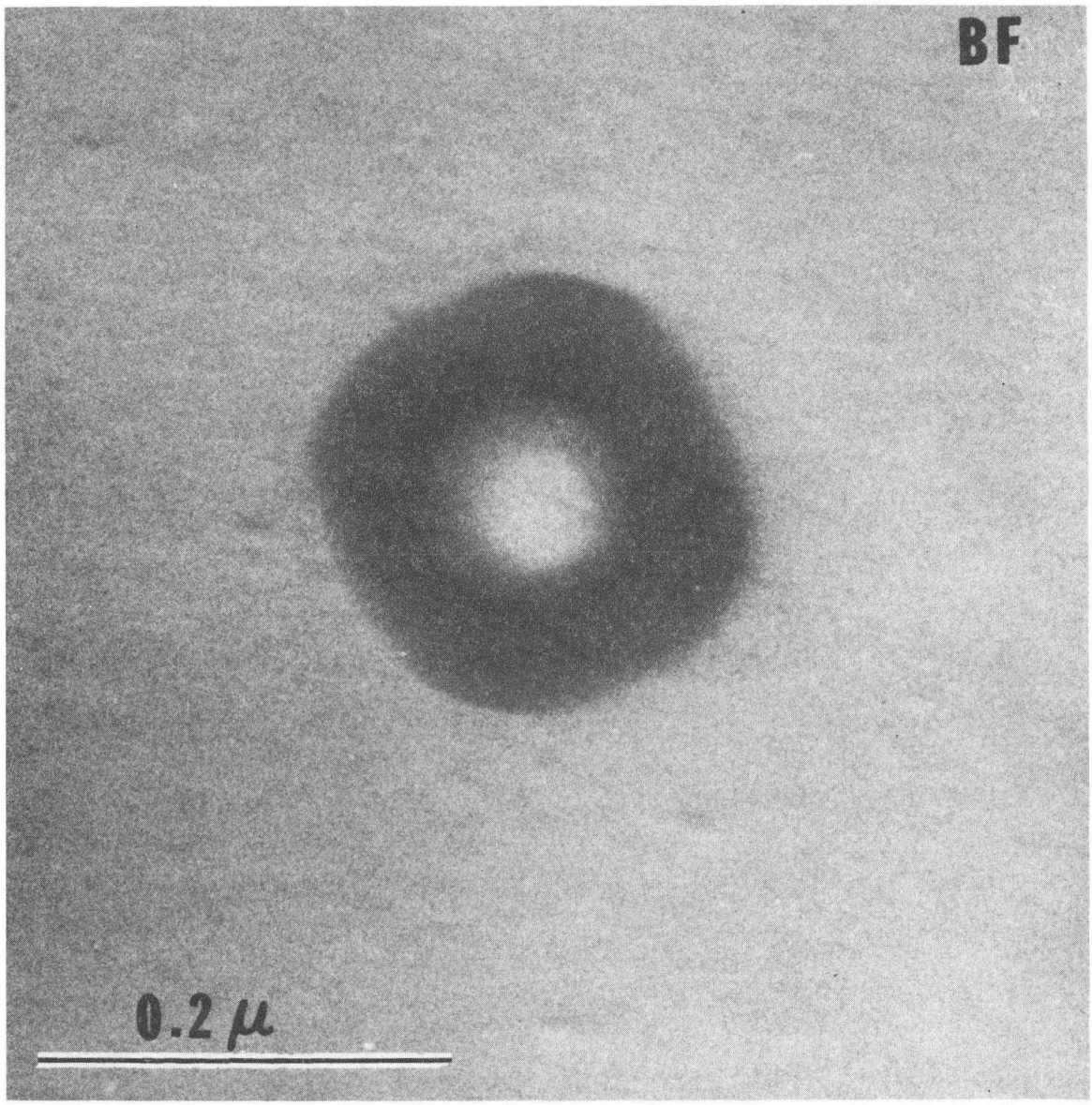

XBB788-9506

Fig. 2a

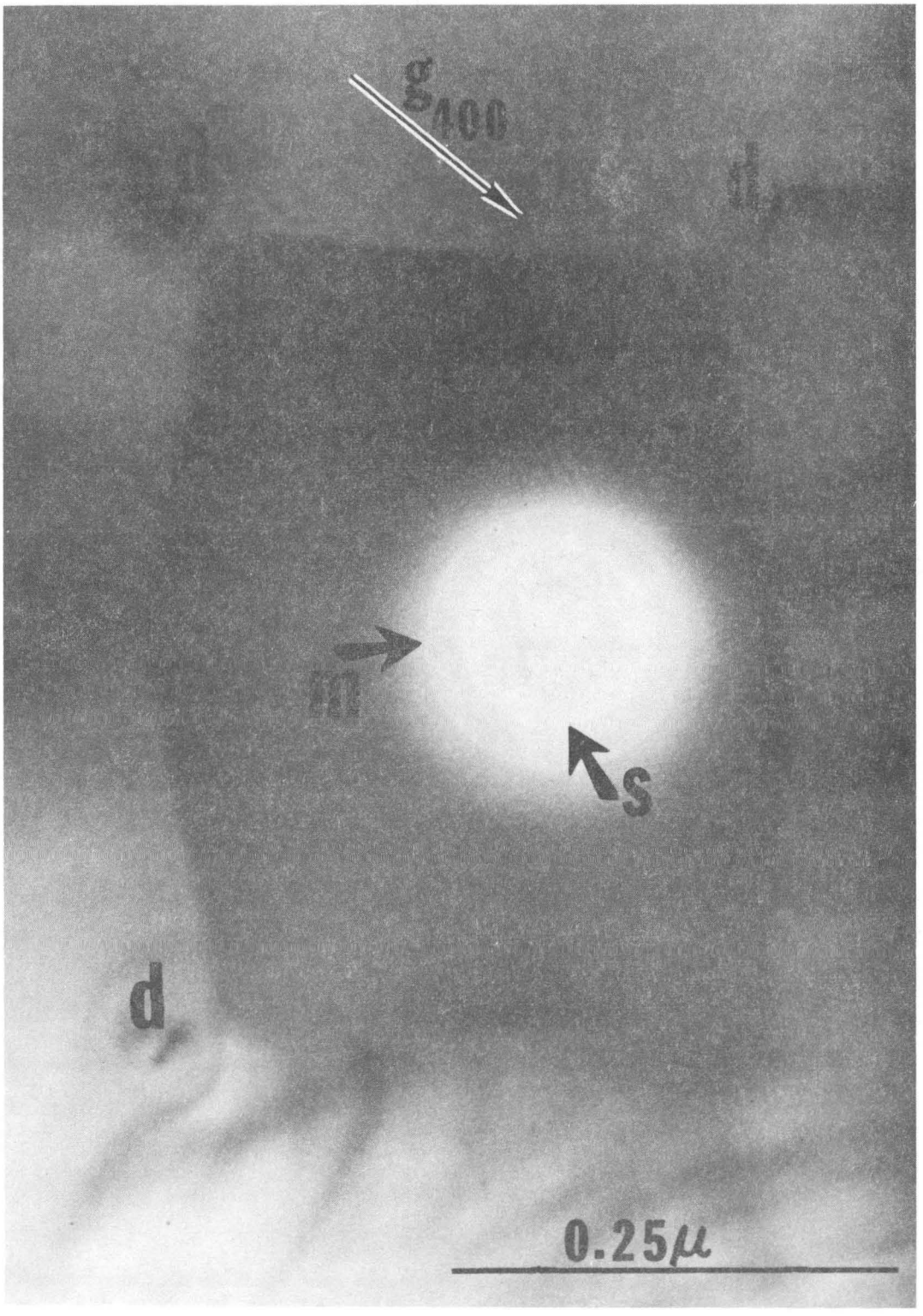

XBB 788-9505

Fig. 2b

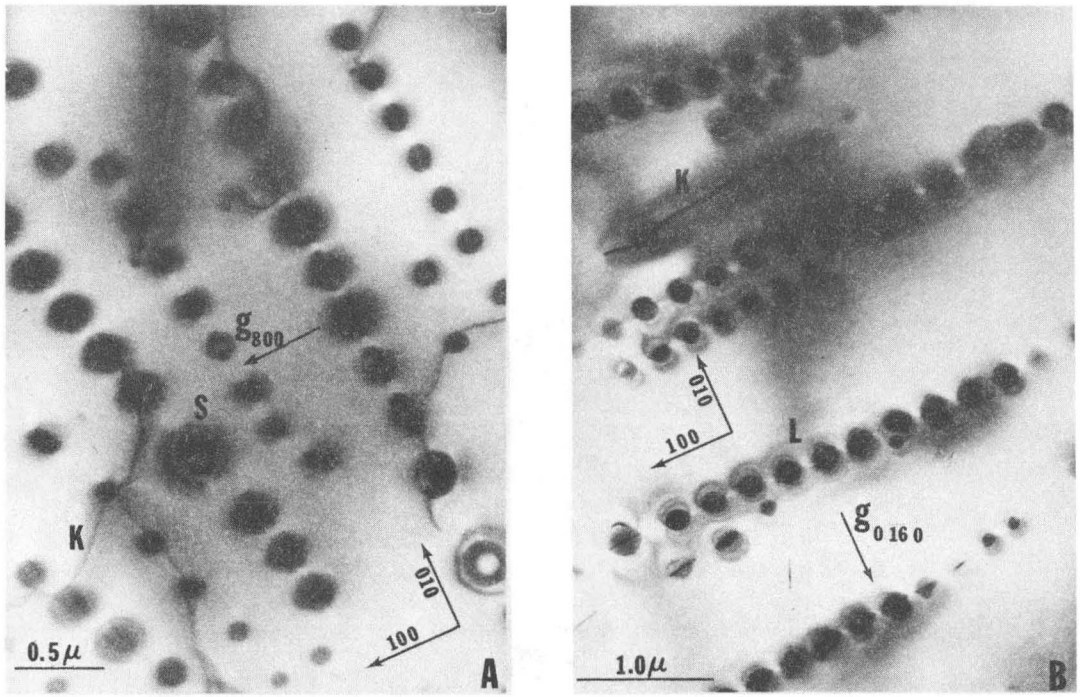

XBB788-9496

Fig. 3

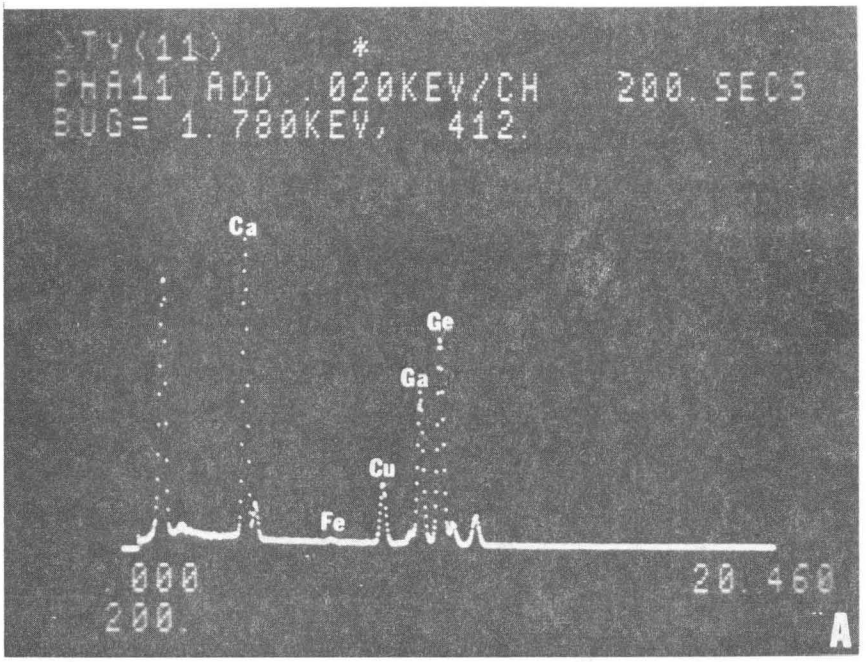

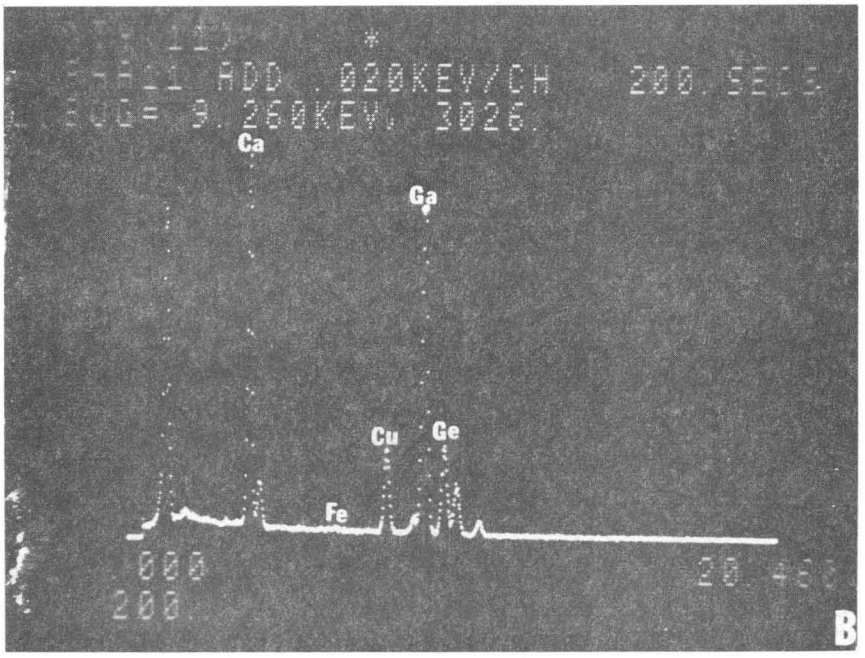

XBB788-9503

Fig. 4

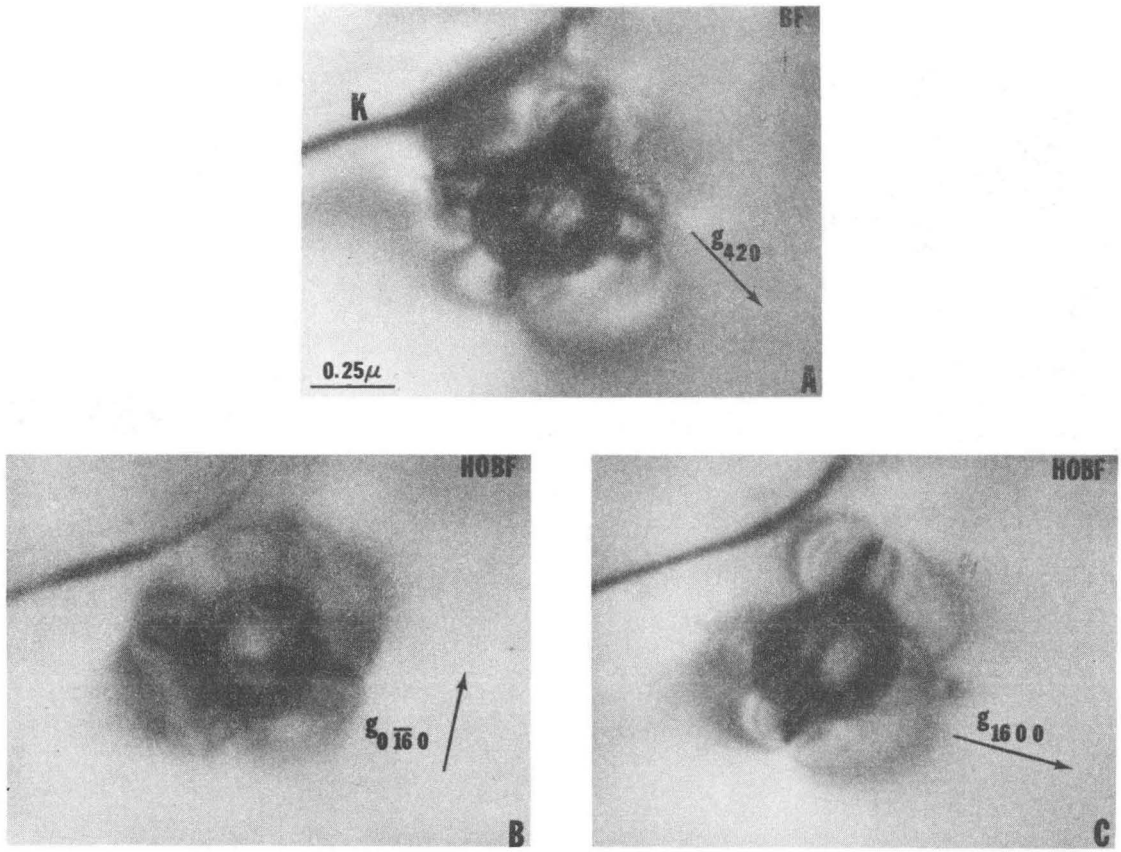

XBB784-4978

Fig. 5

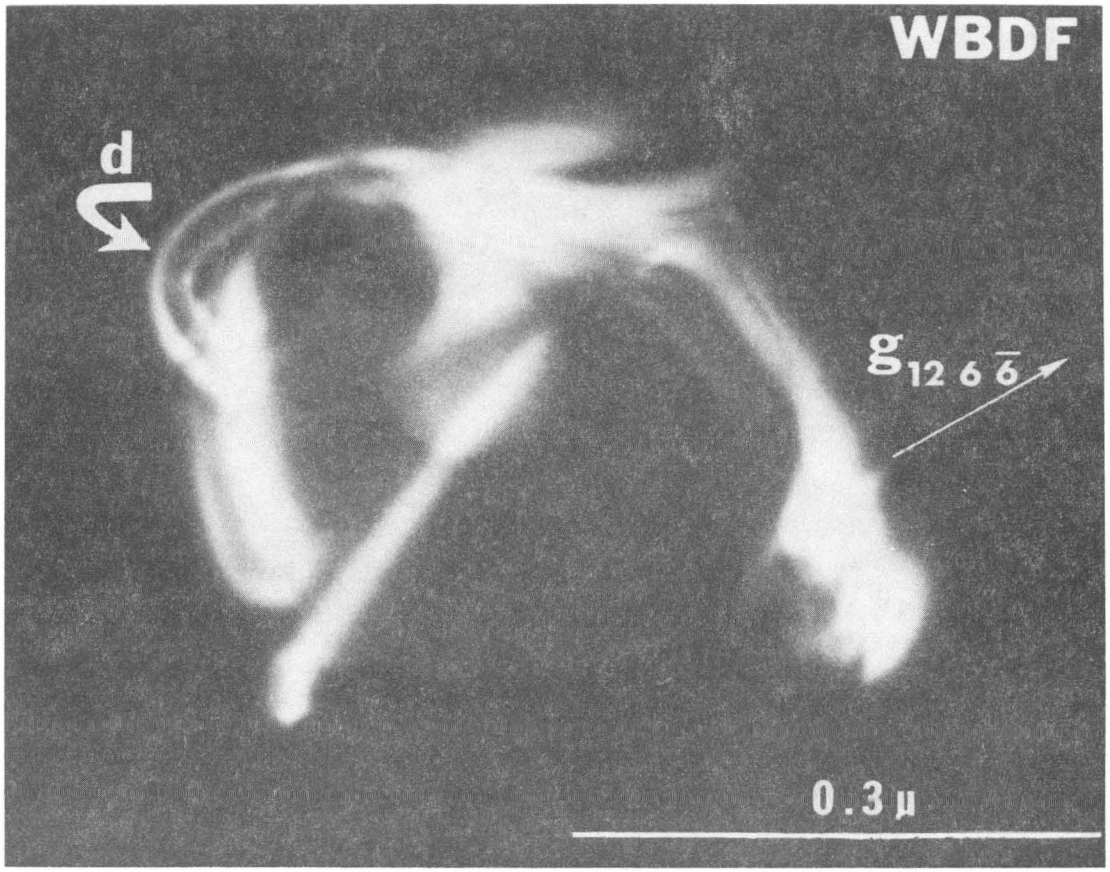

XBB784-4976

Fig. 6

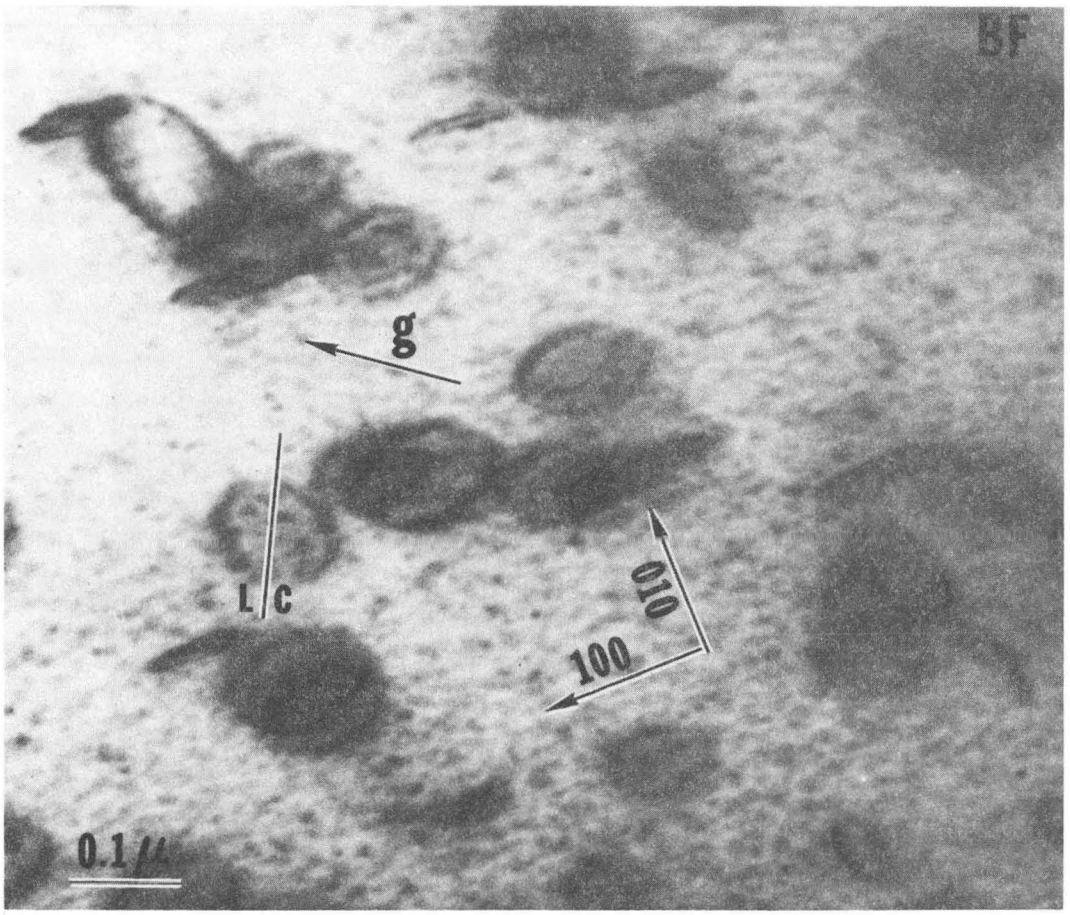

XBB788-9498

Fig. 7a

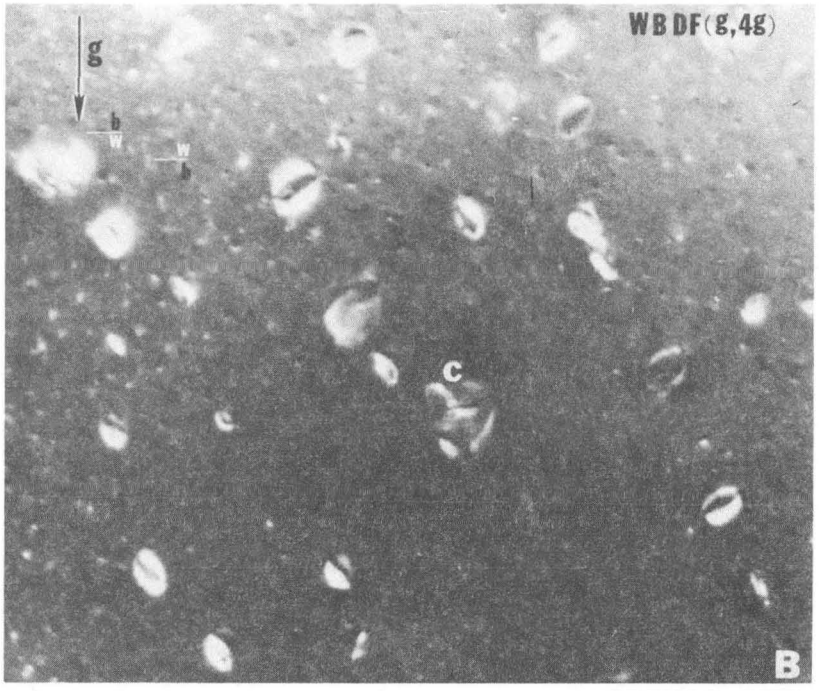

XBB788-9494

Fig. 7b

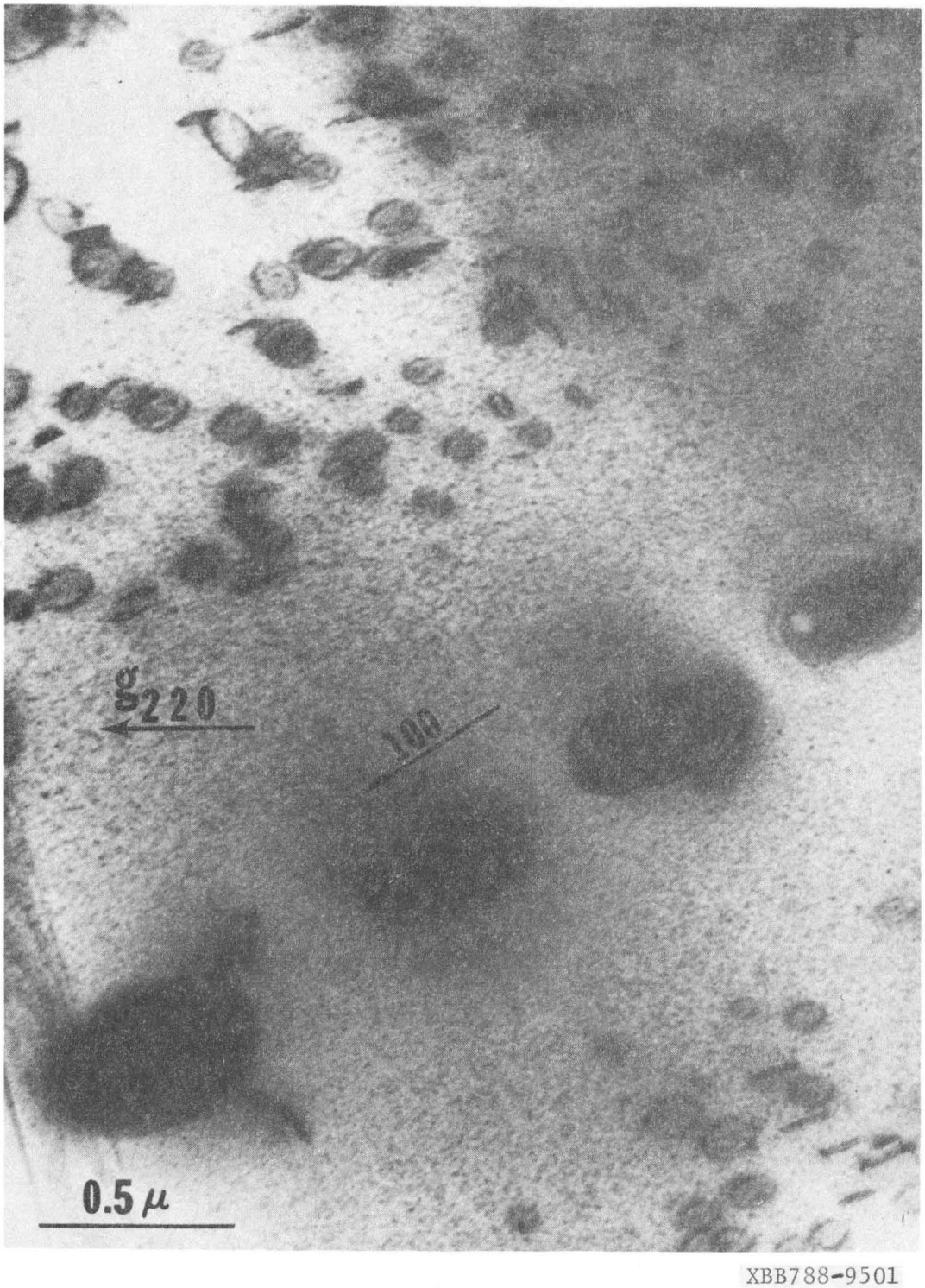

XBB788-9501

Fig. 8

This report was done with support from the Department of Energy. Any conclusions or opinions expressed in this report represent solely those of the author(s) and not necessarily those of The Regents of the University of California, the Lawrence Berkeley Laboratory or the Department of Energy.

Reference to a company or product name does not imply approval or recommendation of the product by the University of California or the U.S. Department of Energy to the exclusion of others that may be suitable.